Atomic-level nature of solid/liquid interface for energy conversion revealed by frequency modulation atomic force microscopy

Minato, Taketoshi ; Umeda, Kenichi ; Kobayashi, Kei ; Araki, Yuki ; Konishi, Hiroaki ; Ogumi, Zempachi ; Abe, Takeshi ; Onishi, Hiroshi ;…

(Citation)
Japanese Journal of Applied Physics,60(SE):SE0806

(Issue Date)
2021-09

(Resource Type)
journal article

(Version)
Version of Record

PROGRESS REVIEW • OPEN ACCESS

Atomic-level nature of solid/liquid interface for energy conversion revealed by frequency modulation atomic force microscopy

To cite this article: Taketoshi Minato *et al* 2021 *Jpn. J. Appl. Phys.* **60** SE0806

OPEN ACCESS

Japanese Journal of Applied Physics **60**, SE0806 (2021) **PROGRESS REVIEW**

https://doi.org/**10.35848/1347-4065/abffa2**

Atomic-level nature of solid/liquid interface for energy conversion revealed by frequency modulation atomic force microscopy

Taketoshi Minato[1*], Kenichi Umeda[2,3], Kei Kobayashi[4], Yuki Araki[5], Hiroaki Konishi[6,7], Zempachi Ogumi[6], Takeshi Abe[8], Hiroshi Onishi[9], and Hirofumi Yamada[4]

[1]*Institute for Molecular Science, National Institutes of Natural Sciences, Nishigonaka 38, Myodaiji-cho, Okazaki, Aichi, 444-8585, Japan*
[2]*Nano Life Science Institute (WPI-NanoLSI), Kanazawa University, Kakumamachi, Kanazawa, Ishikawa 920-1192, Japan*
[3]*PREST/JST, 4-1-8 Honcho, Kawaguchi, Saitama 332-0012, Japan*
[4]*Department of Electronic Science and Engineering, Kyoto University, Nishikyo, Kyoto 615-8510, Japan*
[5]*College of Science and Engineering Department of Physical Sciences, Ritsumeikan University, Nojihigashi 1-1-1, Kusatsu, Shiga 525-8577, Japan*
[6]*Office of Society-Academia Collaboration for Innovation, Kyoto University, Gokasho, Uji, Kyoto 611-0011, Japan*
[7]*Research & Development Group, Hitachi Ltd., Hitachi, Ibaraki 319-1292, Japan*
[8]*Graduate School of Global Environmental Studies, Kyoto University, Katsura, Nishikyo, Kyoto 615-8510, Japan*
[9]*Department of Chemistry, School of Science, Kobe University, Nada-ku, Kobe 657-8501, Japan*

[*]E-mail: minato@ims.ac.jp

Received March 14, 2021; revised April 9, 2021; accepted May 10, 2021; published online July 13, 2021

Understanding and controlling the mechanism of energy conversion related to the development of a sustainable society not only make our lives more convenient but also make them more meaningful and enrichens us. The physical properties at the interface between solid and liquid (solid/liquid interface) play a significant role in energy conversion. The solid/liquid interface is buried and spatially limited, and thus clarifying the physical properties at the interface at the atomic scale is challenging. In this review, we describe our achievements by using frequency modulation atomic force microscopy for studying the geometric structure, molecule distribution, and viscosity at the solid/liquid interface at the atomic scale.

Supplementary material for this article is available online

1. Introduction

The interface between solid and liquid (solid/liquid interface) has several applications in physics, chemistry, and biology, such as electric devices, electrode reactions, catalysis, crystal growth, and cell behavior.[1–3)] Among them, energy conversion reactions occurring at the solid/liquid interface are one of the most important targets for recent scientific research to reduce energy and environmental problems. Rechargeable batteries are significant contributors to current energy technologies. The physical properties and reactions at the interface between the electrode and electrolyte (electrode/electrolyte interface) in rechargeable batteries (Fig. 1) have a strong impact on the battery performance in terms of capacity, rate performance, lifetime, etc.[2)] Traditionally, the analysis of the interface by electrochemical measurements has been used to discuss the physical properties and reaction mechanism. In addition, advanced measurements using light[4–18)] and neutrons[19–21)] have been used to analyze the geometric and electronic structures of the interface. These analyses provide crucial information regarding the interface. In addition to these analyses, atomic analysis of the interface through direct observation using microscopic techniques provides a more detailed understanding of the interface.

The precise analysis of geometric structures,[22–28)] electronic states,[24–26,29)] vibrational states,[30–32)] spin states,[33–35)] and reaction dynamics[36–42)] by scanning probe microscopy (SPM)[22–25)] have been achieved in ultra-high vacuum (UHV). The development of SPM has enabled the analysis of the solid/liquid interface at the atomic scale. Initial analysis of the solid/liquid interface at the atomic scale using SPM, scanning tunneling microscopy (STM) was used in the 1990s.[43)] STM observation at the interface opened a new aspect of the solid/liquid interface

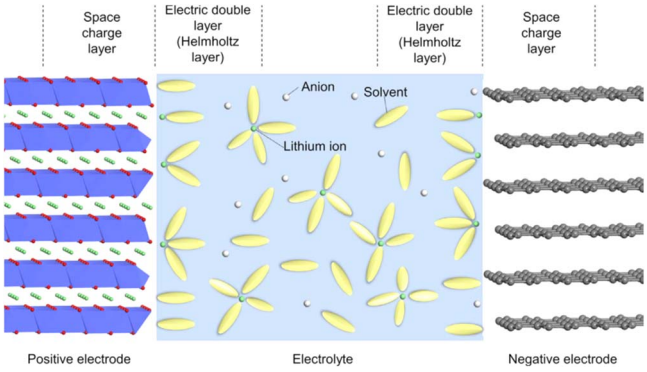

Fig. 1. (Color online) A schematic model of the structure of the interface between electrode and electrolyte in a rechargeable battery (here is a lithium ion battery). The green and white balls denote lithium ions and anions, respectively. The yellow ellipses represent solvent molecules. Positive and negative electrodes having layered structures are shown as a typical example. Reprinted from Ref. 2, Copyright (2017), with permission from Elsevier.

at the atomic scale. The application of STM is limited to conductive solids and is mainly used to observe the geometric structure of a solid surface. Since the 2000s, through the development of experimental techniques for frequency-modulated atomic force microscopy (FM-AFM) in liquid by Yamada et al.,[44,45)] the solid/liquid interface containing insulative solids has been analyzed by AFM at the atomic scale. The specialty of the FM-AFM in liquid is not only to observe the insulator but also to obtain information about the liquid phase at the interface.[44–49)] This is a unique feature of FM-AFM in liquid and is quite difficult to obtain using other methods. The application of FM-AFM to rechargeable battery systems has been a long-term perspective. However, the interfaces in

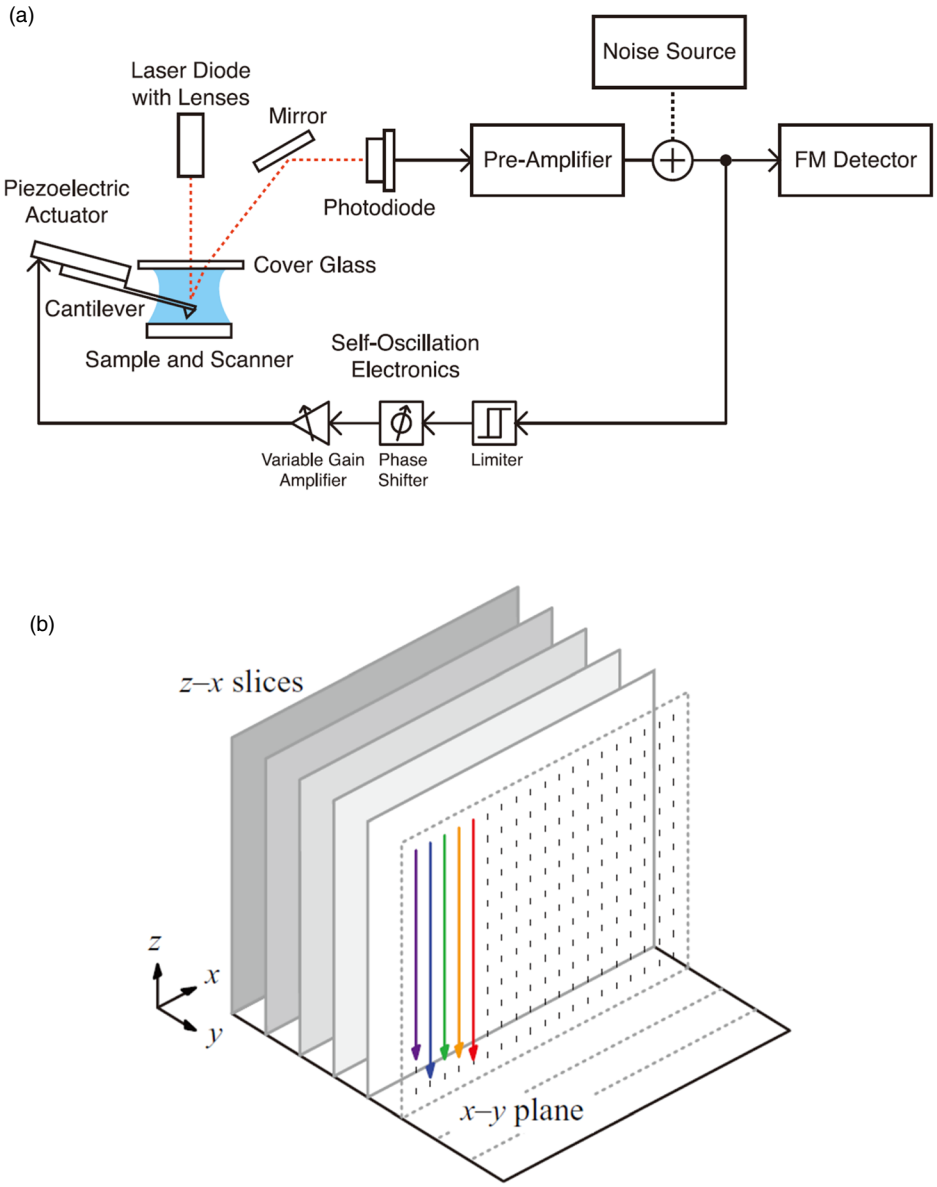

Fig. 2. (Color online) (a) Experimental setup for the FM-AFM in liquid. Reprinted from Ref. 51, with permission of The Japan Society of Applied Physics. The noise source was added to measure the effects of the deflection sensor noise on the frequency noise in Ref. 51. In the setup of usual FM-AFM measurements, the noise source is not used. (b) Basic principle of the 3D measurements. Reprinted from Ref. 52, with the permission of AIP Publishing.

rechargeable batteries are extremely complicated because the electrode is composed of composite materials comprising active materials, conductive materials, and binders.[2)] In addition, electrolytes are complicated and typically composed of organic solvents with inorganic salts and additives.[2)] This hindered a more thorough analysis of the interface.

We analyzed the solid/liquid interface by FM-AFM using precise measurement systems and constructed an appropriate model system to achieve highly sensitive measurements. In this review, our recent approach for analyzing the interface related to the energy conversion system, especially rechargeable batteries, and the future perspective of the FM-AFM analysis are described.

2. Experimental equipment

The experimental system used for the results presented in this review is mainly obtained through FM-AFM, which can operate in liquid environments [Fig. 2(a)].[46–52)] The experimental system was constructed using AFM based on Shimadzu SPM-9600 and 8000FM. The system was constructed using an AFM head with a scanner, electronics, and a controller using a field-programmable gate array programmed with National Instruments LabVIEW. To reduce thermal drift, all experimental systems were placed in an incubator to achieve thermal equilibrium.

In the experimental system, the tip-sample interaction force was detected as the resonance frequency shift (Δf) of the oscillating cantilever. In liquid, the extreme reduction of the Q factor of oscillation by hydrodynamic interactions with the cantilever disturbs the stable oscillation. Yamada et al. developed a system using small amplitude and large noise reduction in a cantilever deflection sensor that permitted FM-AFM operation in liquids (Fig. 2).[51,52)] Atomic resolution in liquid was first achieved by imaging muscovite mica in water using the FM-AFM system.[44)]

The observation of the solid/liquid interface by the FM-AFM system was performed through lateral and vertical scanning for analysis.[52)] For lateral scanning, the vertical tip position of the cantilever was controlled to maintain a constant Δf. Keeping the constant Δf, the cantilever was

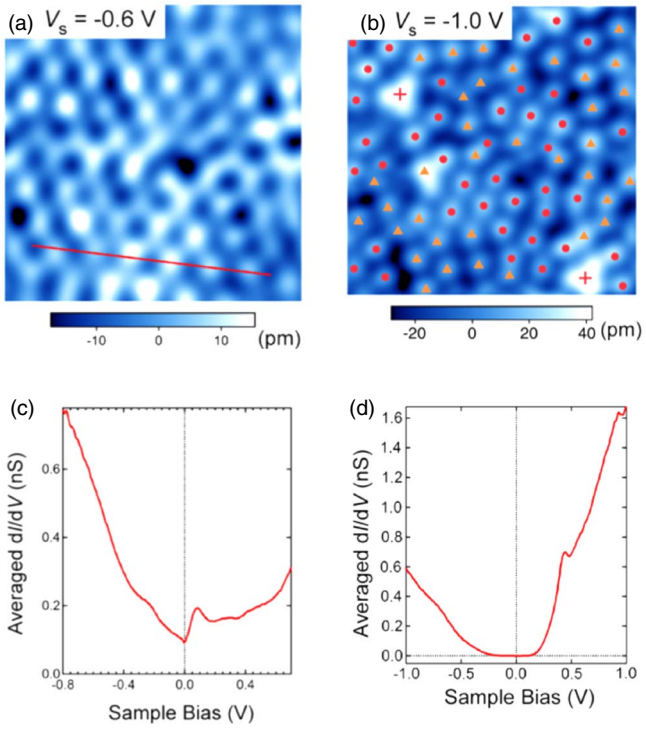

Fig. 3. (Color online) (a) and (b); STM images and (c) and (d); STS spectra obtained at ordered and disordered region on the $Li_{0.66}CoO_2$(001) surface. The sample bias at (a) and (b) are −0.6 and −1.0 V, respectively. The triangles, squares and circles in (b) show the protrusions observed at −1.0 V, +0.8 V and at both sample bias, respectively. Reprinted from Ref. 57 with the permission of American Physical Society.

laterally scanned to obtain a two-dimensional topographic image. In addition, vertical scanning of the cantilever was performed in this AFM system to observe the molecular nature of the liquid phase at the interface. In the 3D mapping, a tip was scanned in Z and XY to cover the entire interface [Fig. 2(b)]. During the vertical scan, Δf was recorded by a 3D Δf image. The efficient scanning of the cantilever allowed us to obtain a 3D image in ∼1 min.

3. Electrode/electrolyte interface for lithium ion battery (LIB)

LIBs are widely used rechargeable batteries in modern life because of their high energy density and excellent cyclic performance.[2,53–56] At the electrode/electrolyte interface in the LIB, carrier ions (Li^+), atoms/ions in the electrode materials, solvents, solute, and additives in the electrolyte form an electric double layer in the liquid phase, and the space charge layer shows characteristic properties that differ from those of the bulk in the solid phase (Fig. 1). The physical properties and reactions at the electrode/electrolyte interface significantly affect the battery performance. However, the electrode/electrolyte interface is an extremely complicated system that is not well understood. In addition, the interface is a spatially constrained region, which causes difficulties in the analysis. Thus, many unclear points at the interface remain. Here, the application of SPM to the analysis of the solid/liquid interface related to LIBs is described.

First, the analysis of the electric structure of the electrode interface at the atomic scale by STM[57] is described. To obtain the physical properties of the interface, an appropriate model system is required. We prepared a single crystal of $Li_{0.66}CoO_2$, which the most widely used material for positive electrodes in LIBs. We used low-temperature STM under UHV conditions to investigate the physical properties at the atomic scale. The local electron conductivity of $Li_{0.66}CoO_2$ was also investigated. By applying a negative sample bias of –0.6 to –1.0 V, the oxygen at the surface with three adjacent Co^{3+} ions on Li vacancy at the subsurface was observed as bright features in STM images [Figs. 3(a) and 3(b), the calculated density of states on the $Li_{0.66}CoO_2$ surface are shown in Fig. S1 available online at stacks.iop.org/JJAP/60/SE0806/mmedia]. In the same sample, different features were observed in the STM images. In a certain region, ordered images with well-aligned bright spots were observed [Fig. 3(a)]; however, disordered images were observed in another region [Fig. 3(b)]. The bright spots were caused by oxygen ions on the Li vacancies. The ordering of the bright spots indicates that the Li vacancies were well aligned. By measuring scanning tunneling spectroscopy (STS) in the two regions, conductive [Fig. 3(c)] and semi-conductive [Fig. 3(d)] spectra were observed in the ordered and disordered regions, respectively. The results showed that the local electron conductivity of Li_xCoO_2 was influenced by the ordering of Li vacancies. To proceed with the charge and discharge processes, the electron conductivity of the electrode should be high, which shows that the ordering of Li vacancies in the electrode enhances the charge and discharge reactions.

The UHV work clarified the new characteristics of the electronic structure of the electrode surface for LIBs. In the next step, FM-AFM in liquid was applied to the model system of the electrode/electrolyte interface. Figure 4 shows a topographic image obtained at the interface between

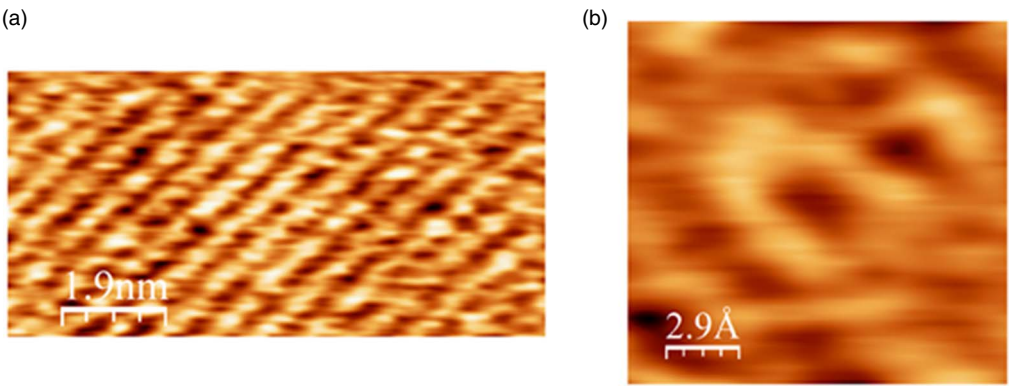

Fig. 4. (Color online) The topographic images of (a) aligned and (b) isolated teraglyme at the tetraglyme/highly oriented pyrolytic graphite (HOPG) interface at $\Delta f = 1000$ Hz. Reprinted from Ref. 58 with the permission of AIP Publishing.

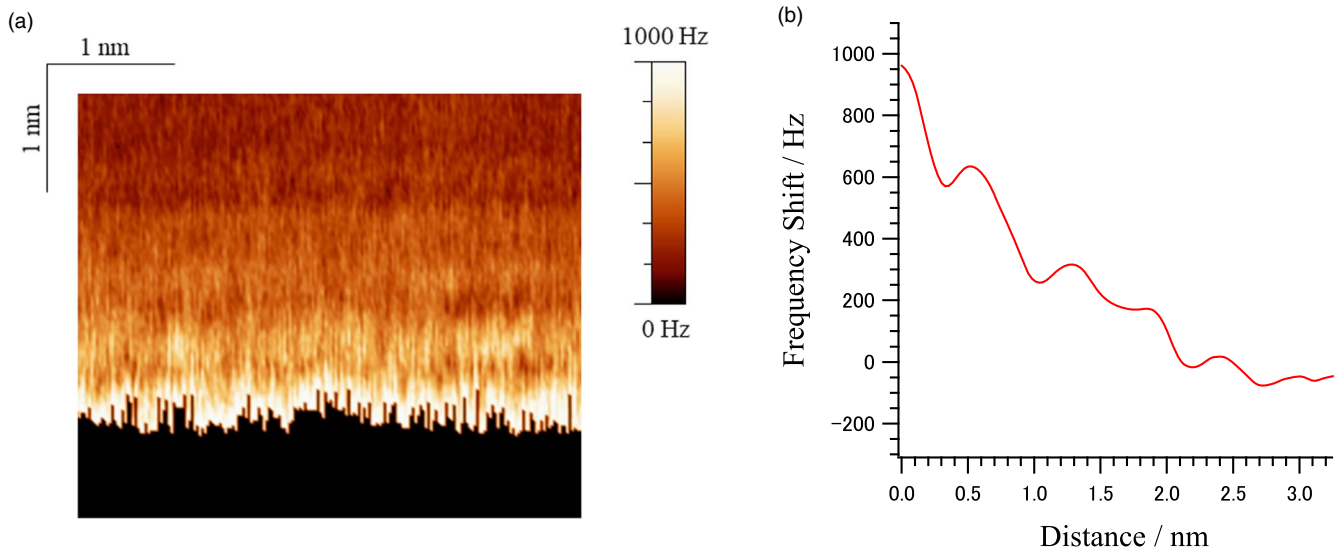

Fig. 5. (Color online) (a) The mapping of cross-sectional Δf distribution and (b) averaged vertical Δf-distance obtained at the HOPG/tetraglyme interface. Reprinted from Ref. 58 with the permission of AIP Publishing.

tetraglyme and graphite (highly oriented pyrolytic graphite (HOPG)).[58] Tetraglyme is a solvent that has been investigated for electrolyte in LIBs. Graphite is a typical material for negative electrodes in LIBs. Although most of the insertion and extraction reactions of Li^+ proceed at the step at the basal plane of HOPG, the surface is used as a model because the component is the same as that of the graphite electrode. In addition, the surface of the basal plane of HOPG is atomically flat and adequate for the detection of quite small signals by FM-AFM. By obtaining the lateral image, a periodic linear structure with a distance of ∼0.62 nm was observed [Fig. 4(a)]. The density functional theory (DFT) calculations showed that tetraglyme adsorbed on the HOPG surface, forming a periodic structure with a distance of ∼0.65 nm, which matches well with the experimentally observed distance between the linear structures (Fig. S2). This suggests that the observed periodic structure was caused by the tetraglyme molecules adsorbed on the HOPG surface. Further, we observed a characteristic U-like structure in the topographic images [Fig. 4(b)]. DFT calculations also support that the U-like structure is caused by the adsorption of the isolated tetraglyme molecule on HOPG (Fig. S3). Thus, the isolated molecules at the interface were directly observed using FM-AFM. These results show that the molecular resolution was achieved at the interface. The molecular nature around the interface in the liquid phase was analyzed by monitoring the frequency shift (Δf) during a vertical scan of the cantilever. From the Δf distribution, four peaks with an average distance of 0.60 nm were observed at the interface [Figs. 5(a) and 5(b)]. The layered structure is attributed to the high density of tetraglyme molecules around the interface due to the interaction between tetraglyme and the HOPG surface (Fig. S4). From the lateral and vertical images, a schematic model of the interface structure between tetraglyme and HOPG was proposed. As is well known, the molecular structure and distribution of the electrode/electrolyte interface strongly affect the battery performance. The strong interaction between tetraglyme and graphite affects the insertion and extraction of Li^+. This work provided us with the possibility to observe the electrode/electrolyte interface in rechargeable batteries directly at the atomic/molecular scale. Further investigations will show the true nature of the interface in working batteries.

4. Viscosity distribution at the solid/liquid interface

During the chemical reactions at the solid/liquid interface, the reaction occurs by the attack of atoms (or molecules and ions) in the liquid to the solid surface. The viscosity of the liquid phase strongly influences the reaction mechanism because the frequency of the attack depends on the viscosity of the liquid phase. In particular, at the electrode/electrolyte interface in a rechargeable battery, the insertion and extraction of carrier ions are strongly influenced by the viscosity. Diffusivity measurement by NMR is widely used; however, it is not a spatially resolved method.[59] Visualization of the viscosity at the solid/liquid interface at the atomic scale significantly enhances the understanding of the true nature of the interface.

In the FM-AFM measurements, a dissipative damping signal for the oscillation of the cantilever was detected. The origin of the damping signal in the FM-AFM measurement is regarded as the hysteresis between the approaching and retracting of the cantilever and is caused by rearrangements of the tip-sample atoms in UHV work.[60–63] In a liquid, the rearrangements are directly related to the local viscosity of the liquid. Viscosity mapping can be achieved by mapping dissipative damping at the solid/liquid interface. However, quantitative detection of the dissipative damping signal in the liquid was not achieved. In our FM-AFM measurements, the dissipative damping signal can be decoupled and separately detected from Δf, which is caused by the conservative force. Figures 6(a) and 6(b) show the 3D mapping images obtained by simultaneous measurements of the conservative force calculated from the observed Δf and the dissipative damping signal at the interface between $CaCO_3$ and water.[47] The lateral mapping at the interface of the conservative force and dissipative damping signals extracted from the 3D data in

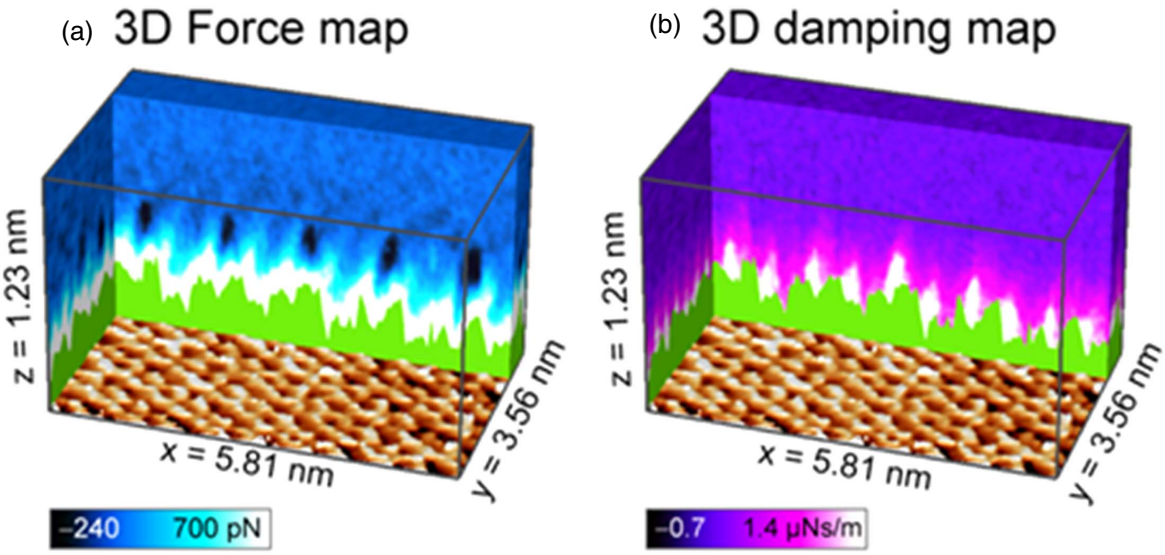

Fig. 6. (Color online) 3D mapping of conservative force (b) and damping (c) maps obtained at the $CaCO_3$/water interface. Reprinted from Ref. 47 with the permission of the American Physical Society.

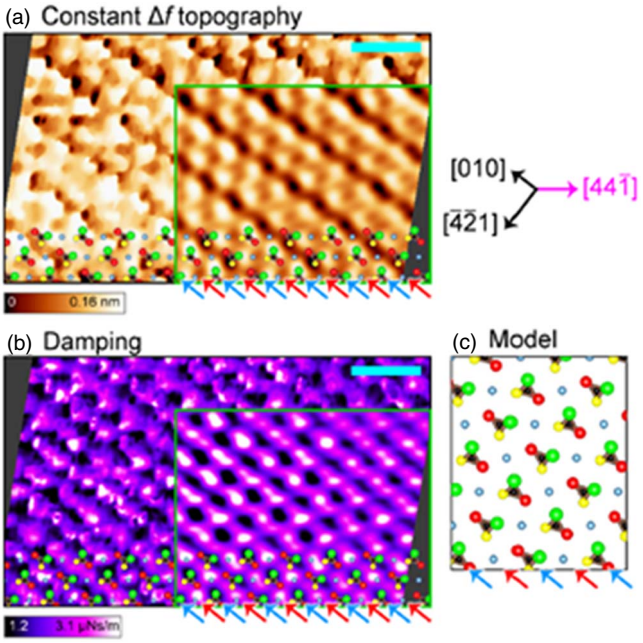

Fig. 7. (Color online) (a)–(c) Experimental reconstructed topography (b) and damping image (b) at $\Delta f = 4$ kHz and crystal structure (c). The scale bars are 1 nm in (a) and (b). Reprinted from Ref. 47 with the permission of the American Physical Society.

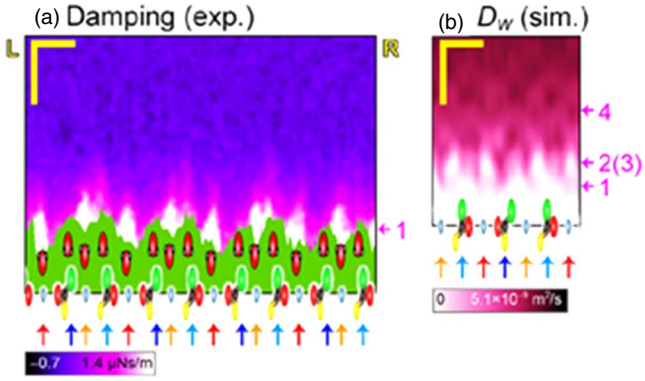

Fig. 8. (Color online) Site dependencies of (a) dissipative damping and (b) simulated D_w obtained at the $CoCO_3$/water interface. To compare (a) and (b) easily, the contrast of D_w is shown; a brighter (darker) signal reflects smaller (higher) D_w. Reprinted from Ref. 47 with the permission of the American Physical Society.

Figs. 6(a) and 6(b) at $\Delta f = 4$ kHz are also shown in Figs. 7(a) and 7(b). Based on previous reports of FM-AFM images of $CaCO_3$,[64–67] the bright spots in the conservative force image are assigned as oxygen sites [green ball in Fig. 7(a)]. In contrast, the dissipative damping image showed bright spots at Ca sites [aqua ball in Fig. 7(b)]. Figure 8(a) shows a cross-sectional image of the dissipative damping signal extracted from the 3D data in Fig. 6(b). The calcium sites (aqua ellipses) clearly show higher dissipative damping signals than oxygen sites (green ellipses). This implies that the viscosity at the Ca sites was higher than that at the oxygen sites. To confirm the interpretation of the experimental results, the self-diffusion coefficient (D_w) of water molecules in the liquid was estimated by molecular dynamics calculations using the Einstein relation[47] and is shown as mapping data in Fig. 8(b). The calculated data [Fig. 8(b)] show a tendency similar to that of the experimentally obtained data [Fig. 8(a)]. This confirms that the 3D mapping of viscosity at the solid/liquid interface was achieved by FM-AFM measurements. On the $CaCO_3$ surface, the Ca sites are slightly dented by the surrounding oxygen of CO_3. This local environment is thought to increase the viscosity of water molecules. In addition, the positive charge at the Ca sites strongly interacts with water molecules due to the dipole moment and increases the viscosity. These factors are the main reasons for the increase in the viscosity at the Ca sites. This work opened new possibilities for observing viscosity at the solid/liquid interface at the atomic scale. As explained previously, the viscosity distribution has a strong impact on the reactions at

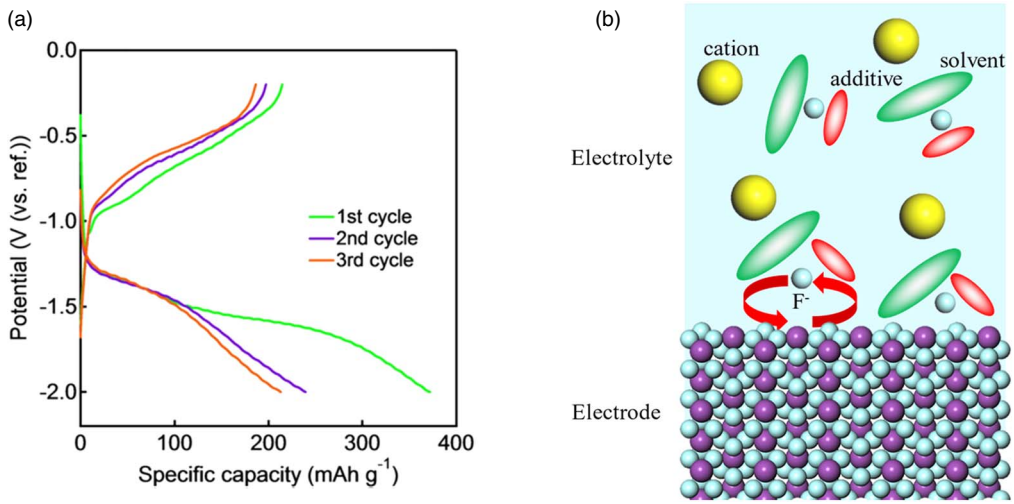

Fig. 9. (Color online) (a) Charge and discharge curves of BiF_3 electrode for the fluoride shuttle battery reaction. Reprinted from Ref. 78 with the permission of Wiley. (b) A schematic model of the electrode/electrolyte interface in fluoride shuttle battery. Purple, aqua, yellow balls are metal, fluoride ions and cations. Green and red ellipses are solvent and additives in electrolyte.

the electrode/electrolyte interface in rechargeable batteries. The analytical technique will be extended to energy conversion systems such as rechargeable batteries in the near future.

5. Future outlook of the application of FM-AFM to energy conversion

As described above, direct observation and analysis of the solid/liquid interface related to rechargeable batteries can be achieved through FM-AFM. However, in an in situ analysis, analysis during the charge and discharge reactions of the interface still cannot be achieved. In the case of amplitude-modulation AFM, in situ analysis has already been reported,[68] and the formation of SEI or change of the active materials is observed. Experimentally, electrochemical FM-AFM measurements were reported by Fukui, Utsunomiya and Yokota.[69] A more detailed mechanism will be elucidated by atomic-scale analysis using FM-AFM during the charge and discharge reactions.

AFM will be further extended to new energy conversion systems that can overcome current energy technologies. LIBs are the most widely used rechargeable batteries; however, the recent demand for rechargeable batteries has necessitated improvements in battery performance. Fluoride shuttle battery (FSB) is a new battery based on the shuttle of fluoride ions in the electrolyte and theoretically overcomes the energy density of current LIB.[69–75] It has a much higher theoretical energy density than the current battery systems.[74–76] The charge and discharge reactions of this battery system have been reported in solid electrolyte systems operating at high temperatures (~150 °C).[70,74,76] Recently, liquid electrolytes for FSB working at room temperature have been developed.[71,72,75,77] Figure 9(a) shows the charge-discharge curve of the BiF_3 electrode in a liquid electrolyte prepared from CsF, triphenylboroxine (TPhBX), and tetraglyme.[78] Reversible capacities were observed in the liquid electrolyte at room temperature. Organic electrolytes prepared with anion acceptors (AAs) of fluorobis(2,4,6-trimethylphenyl)borane (FBTMPhB),[71,79–82] triphenylborane (TPhB),[82–85] 2,4,6-tris(4-fluorophenyl) boroxine (TFPhBX),[86] TPhBX,[78,82–84,87–89] and lithium bis (oxalato)borate (LiBOB)[90,91] have been reported. For the active materials of electrodes working in a liquid containing AA electrolyte, BiF_3[71,72,77,79,80,82,84,90,91] and PbF_2[72,81,83,85,88] have been reported. The fluorination and defluorination of the electrode are enhanced by a mixture of active materials with conductive materials[80,88] and BaF_2.[81] The chemical reactions occurring at the electrode/electrolyte interface [Fig. 9(b)] in FSB are quite sensitive to the components of the liquid electrolyte.[80,82,87] The liquid electrolyte was designed to have an appropriate interaction of fluoride ion with the electrode to proceed with fluorination and defluorination. However, the reactions occurring at the interface have many ambiguities. AFM analysis at the electrode/electrolyte interface will be useful for understanding the reaction and developing an FSB system.

6. Conclusions

FM-AFM in liquids can visualize the solid/liquid interface in 3D and clarify the physical properties and reaction mechanism of the energy conversion at the solid/liquid interface. In this review, our achievements in the analysis of the geometric structure, molecular distribution, and viscosity at the solid/liquid interface are described. Further developments of the experimental techniques for in situ measurements during charge and discharge reactions and their application to new energy conversion systems will clarify new faces of the solid/liquid interface.

Acknowledgments

Part of the research described in this review was supported by the "Research and Development Initiative for Scientific Innovation of New Generation Batteries (RISING)," JPNP09012 and "Research and Development Initiative for Scientific Innovation of New Generation Batteries (RISING2)," JPNP16001, commissioned by the New Energy and Industrial Technology Development Organization (NEDO), Japan.

ORCID iDs

Taketoshi Minato https://orcid.org/0000-0002-5443-1709

1) D. P. Woodruff, *The Solid-Liquid Interface* (Cambridge University Press, Cambridge, 1973) Solid State Science Series.
2) T. Minato and T. Abe, Prog. Surf. Sci. **92**, 240 (2017).
3) K Wandelt, *Surface and Interface Science* (Wiley, New York, 2020) Liquid and Biological Interfaces, Vol. 7.
4) P. Fenter and N. C. Sturchio, Prog. Surf. Sci. **77**, 171 (2004).
5) M. Hirayama et al., J. Power Sources **168**, 493 (2007).
6) M. Mezger et al., Science **322**, 424 (2008).
7) K. Sakamoto, M. Hirayama, N. Sonoyama, D. Mori, A. Yamada, K. Tamura, J. Mizuki, and R. Kanno, Chem. Mater. **21**, 2632 (2009).
8) D. Takamatsu, Y. Koyama, Y. Orikasa, S. Mori, T. Nakatsutsumi, T. Hirano, H. Tanida, H. Arai, Y. Uchimoto, and Z. Ogumi, Angew. Chem. Int. Ed. **51**, 11597 (2012).
9) K. Yamamoto et al., Electrochemistry **82**, 891 (2014).
10) Y. Orikasa et al., Adv. Mater. Interfaces **1**, 1400195 (2014).
11) K. Yamamoto et al., J. Phys. Chem. C **118**, 9538 (2014).
12) D. Takamatsu et al., J. Phys. Chem. C **119**, 9791 (2015).
13) M. Matsui, K. Dokko, and K. Kanamura, J. Power Sources **177**, 184 (2008).
14) K. Motobayashi, K. Minami, N. Nishi, T. Sakka, and M. Osawa, Phys. Chem. Chem. Phys. **4**, 3110 (2013).
15) J. P. Vivek, N. Berry, G. Papageorgiou, R. J. Nichols, and L. J. Hardwick, J. Am. Chem. Soc. **138**, 3745 (2016).
16) H. Liu, Y. Tong, N. Kuwata, M. Osawa, J. Kawamura, and S. Ye, J. Phys. Chem. Lett. **113**, 20531 (2009).
17) L. Yu, H. Liu, Y. Wang, N. Kuwata, M. Osawa, J. Kawamura, and S. Ye, Angew. Chem. Int. Ed. **52**, 5753 (2013).
18) P. Mukherjee, A. Lagutchev, and D. D. Dlott, J. Electrochem. Soc. **159**, A244 (2012).
19) J. E. Owejan, J. P. Owejan, S. C. DeCaluwe, and J. A. Dura, Chem. Mater. **24**, 2133 (2012).
20) G. M. Veith, L. Baggetto, R. L. Sacci, R. R. Unocic, W. E. Tenhaeff, and J. F. Browning, Chem. Commun. **50**, 3081 (2014).
21) T. Minato et al., J. Phys. Chem. C **120**, 20082 (2016).
22) G. Binning, H. Rohrer, C. Gerber, and E. Weibel, Phys. Rev. Lett. **49**, 57 (1982).
23) G. Binnig, H. Rohrer, C. Gerber, and E. Weibel, Phys. Rev. Lett. **50**, 120 (1983).
24) R. Wiesendanger, *Scanning Probe Microscopy and Spectroscopy* (Cambridge University Press, Cambridge, 1994).
25) D. Bonnell, *Scanning Probe Microscopy and Spectroscopy* (Wiley, New York, 2001).
26) T. Minato, Chem. Rec. **14**, 923 (2014).
27) M. Feng, J. Zhao, and H. Petek, Science **320**, 359 (2008).
28) T. Minato, T. Susaki, S. Shiraki, H. S. Kato, M. Kawai, and K.-I. Aika, Surf. Sci. **566**, 1012 (2004).
29) T. Minato et al., J. Chem. Phys. **130**, 124502 (2009).
30) B. C. Stipe, M. A. Rezaei, and W. Ho, Science **280**, 1732 (1998).
31) Y. Kim, T. Komeda, and M. Kawai, Phys. Rev. Lett. **89**, 126104 (2002).
32) P. Hapala, R. Temirov, F. S. Tautz, and P. Jelinek, Phys. Rev. Lett. **113**, 226101 (2014).
33) V. Madhavan, W. Chen, T. Jamneala, M. F. Crommie, and N. S. Wingreen, Science **280**, 567 (1998).
34) R. Wiesendanger, Rev. Mod. Phys. **81**, 1495 (2009).
35) H. Gonzalez-Herrero, J. M. Gomez-Rodriguez, P. Mallet, M. Moaied, J. J. Palacios, C. Salgado, M. M. Ugeda, J. Y. Veuillen, F. Yndurain, and I. Brihuega, Science **352**, 437 (2016).
36) D. M. Eigler, C. P. Lutz, and W. E. Rudge, Nature **352**, 600 (1991).
37) B. C. Stipe, M. A. Rezaei, and W. Ho, Science **279**, 1907 (1998).
38) T. Minato, M. Kawai, and Y. Kim, J. Mater. Res. **27**, 2237 (2012).
39) T. Minato, N. Asao, Y. Yamamoto, M. Kawai, and Y. Kim, Chem. Lett. **42**, 942 (2013).
40) H. Petek, ACS Nano **8**, 5 (2014).
41) T. Minato, S. Kajita, C.-L. Pang, N. Asao, Y. Yamamoto, T. Nakayama, M. Kawai, and Y. Kim, ACS Nano **9**, 6837 (2015).
42) Y. Kim, K. Motobayashi, T. Frederiksen, H. Ueba, and M. Kawai, Prog. Surf. Sci. **90**, 85 (2015).
43) K. Itaya, Prog. Surf. Sci. **58**, 121 (1998).
44) T. Fukuma, T. Ichii, K. Kobayashi, H. Yamada, and K. Matsushige, Appl. Phys. Lett. **87**, 034101 (2005).
45) T. Fukuma, Y. Ueda, S. Yoshioka, and H. Asakawa, Phys. Rev. Lett. **104**, 016101 (2010).
46) K. Umeda, K. Kobayashi, T. Minato, and H. Yamada, Langmuir **34**, 9114 (2018).
47) K. Umeda, K. Kobayashi, T. Minato, and H. Yamada, Phys. Rev. Lett. **122**, 116001 (2019).
48) K. Umeda, K. Kobayashi, T. Minato, and H. Yamada, J. Phys. Chem. Lett. **11**, 1343 (2020).
49) K. Umeda, K. Kobayashi, T. Minato, and H. Yamada, J. Phys. Chem. Lett. **11**, 8094 (2020).
50) K. Kobayashi, H. Yamada, H. Itoh, T. Horiuchi, and K. Matsushige, Rev. Sci. Instrum. **72**, 4383 (2001).
51) H. Yamada, K. Kobayashi, T. Fukuma, Y. Hirata, T. Kajita, and K. Matsushige, Appl. Phys. Express **2**, 095007 (2009).
52) K. Kobayashi, N. Oyabu, K. Kimura, S. Ido, K. Suzuki, T. Imai, K. Tagami, M. Tsukada, and H. Yamada, J. Chem. Phys. **138**, 184704 (2013).
53) G.-A. Nazari and G. Pistoia, *Lithium Batteries* (Springer, Berlin, 2003).
54) M. Yoshio, R. J. Brodd, and A. Kozawa, *Lithium-Ion Battery* (Springer, Berlin, 2009).
55) K. Ozawa, *Lithium Ion Rechargeable Batteries* (Wiley, New York, 2009).
56) B. Scrosati, K. M. Abram, W. Schalkwijk, and J. Hassoum, *Lithium Batteries* (Wiley, New York, 2013).
57) K. Iwaya, T. Ogawa, T. Minato, K. Miyoshi, J. Takeuchi, A. Kuwabara, H. Moriwake, Y. Kim, and T. Hitosugi, Phys. Rev. Lett. **111**, 126104 (2013).
58) T. Minato, Y. Araki, K. Umeda, T. Yamanaka, K.-I. Okazaki, H. Onishi, T. Abe, and Z. Ogumi, J. Chem. Phys. **147**, 124701 (2017).
59) C. P. Slichter, *Principles of Magnetic Resonance* (Springer, Berlin, 1996).
60) N. Sasaki and M. Tsukada, Jpn. J. Appl. Phys. **39**, L1334 (2000).
61) L. N. Kantorovich and T. Trevethan, Phys. Rev. Lett. **93**, 236102 (2004).
62) N. Oyabu, P. Pou, Y. Sugimoto, P. Jelinek, M. Abe, S. Morita, R. Perez, and O. Custance, Phys. Rev. Lett. **96**, 106101 (2006).
63) S. A. Ghasemi, S. Goedecker, A. Baratoff, T. Lenosky, E. Meyer, and H. J. Hug, Phys. Rev. Lett. **100**, 236106 (2008).
64) S. Rode, N. Oyabu, K. Kobayashi, H. Yamada, and A. Kühnle, Langmuir **25**, 2850 (2009).
65) P. Rahe, J. Schütte, and A. Kühnle, J. Phys.: Condens. Matter **24**, 084006 (2012).
66) H. Imada, K. Kimura, and H. Onishi, Langmuir **29**, 10744 (2013).
67) T. Fukuma, B. Reischl, N. Kobayashi, P. Spijker, F. F. Canova, K. Miyazawa, and A. S. Foster, Phys. Rev. B **92**, 155412 (2015).
68) S.-K. Jeong, M. Inaba, T. Abe, and Z. Ogumi, J. Electrochem. Soc. **148**, A989 (2001).
69) K. Fukui, T. Utsunomiya, and Y. Yokota, Jpn. J. Appl. Phys. **56**, 08LA03 (2017).
70) M. A. Reddy and M. Fichtner, J. Mater. Chem. **21**, 17059 (2011).
71) H. Konishi, T. Minato, T. Abe, and Z. Ogumi, J. Electrochem. Soc. **164**, A3702A3708 (2017).
72) K. Okazaki, Y. Uchimoto, T. Abe, and Z. Ogumi, ACS Energy Lett. **2**, 1460 (2017).
73) V. K. Davis et al., Science **362**, 1144 (2018).
74) F. Gschwind, G. Rodriguez Garcia, D. J. S. Sandbeck, A. Gross, M. Weil, M. Fichtner, and N. Gormann, J. Fluor. Chem. **182**, 76 (2016).
75) T. Minato, H. Konishi, A. C. Kucuk, T. Abe, and Z. Ogumi, Ceram. Jpn. **54**, 637 (2019).
76) H. Nakano et al., Chem. Mater. **33**, 459 (2021).
77) M. Kawasaki, K.-I. Morigaki, G. Kano, H. Nakamoto, R. Takekawa, J. Kawamura, T. Minato, T. Abe, and Z. Ogumi, J. Electrochem. Soc. **168**, 010529 (2021).
78) H. Konishi, T. Minato, T. Abe, and Z. Ogumi, ChemistrySelect **5**, 6237 (2020).
79) H. Konishi, A. C. Kucuk, T. Minato, T. Abe, and Z. Ogumi, J. Electroanal. Chem. **839**, 173 (2019).
80) H. Konishi, T. Minato, T. Abe, and Z. Ogumi, J. Appl. Electrochem. **48**, 1205 (2018).
81) H. Konishi, T. Minato, T. Abe, and Z. Ogumi, J. Electroanal. Chem. **826**, 60 (2018).
82) H. Konishi, R. Takekawa, T. Minato, Z. Ogumi, and T. Abe, Chem. Phys. Lett. **755**, 137785 (2020).
83) H. Konishi, T. Minato, T. Abe, and Z. Ogumi, J. Electroanal. Chem. **871**, 114103 (2020).
84) H. Konishi, T. Minato, T. Abe, and Z. Ogumi, Chem. Lett. **47**, 1346 (2018).
85) H. Konishi, T. Minato, T. Abe, and Z. Ogumi, ChemistrySelect **4**, 5984 (2019).

86) H. Konishi, T. Minato, T. Abe, and Z. Ogumi, ChemistrySelect **5**, 4943 (2020).
87) H. Konishi, T. Minato, T. Abe, and Z. Ogumi, J. Phys. Chem. C **123**, 10246 (2019).
88) H. Konishi, T. Minato, T. Abe, and Z. Ogumi, Mater. Chem. Phys. **226**, 1 (2019).
89) Y. Takabayashi et al., Phys. Status Solidi B **257**, 2000202 (2020).
90) A. C. Kucuk, T. Minato, T. Yamanaka, and T. Abe, J. Mater. Chem. A **7**, 8559 (2019).
91) A. C. Kucuk, T. Yamanaka, T. Minato, and T. Abe, J. Electrochem. Soc. **167**, 120508 (2020).